Optimal Trajectory for a Microrobot Navigating in Blood Vessels

Laurent Arcèse, Ali Cherry, Matthieu Fruchard, Antoine Ferreira

Optimal trajectory for a microrobot navigating in blood vessels

Laurent Arcese, Ali Cherry, Matthieu Fruchard, Antoine Ferreira

***Abstract*— The chemotherapy magnetically controlled under Magnetic Resonance Imaging (MRI) is currently one of the active areas of cancer research. This paper proposes a precise model of a therapeutic microrobot magnetically steered in blood vessels. This modeling approach takes into account the non-newtonian behavior of blood, as well as wall effect on the blood's profile and robot-to-wall interaction forces. A backstepping approach law is used to ensure a null error between the real trajectory and an optimal reference trajectory deduced from the highly nonlinear model. The strengths and limitations of the overall study are evaluated by simulations.**

I. INTRODUCTION

Cancer is a class of diseases in which a group of cells display uncontrolled growth, invasion, and sometimes metastasis. Since complete eradication of cancer cells is imperative, total excision is the best treatment. However, depending on the tumor location and the damage caused to surrounding tissues, surgery is not always possible. In these conditions, chemo or radiotherapy becomes necessary. The drawback of these treatments is that they do not differentiate between healthy and diseased cells. Therefore, the development of techniques that could selectively deliver drug molecules to the diseased site, and among them the chemotherapy magnetically controlled under MRI, is currently a promising area of cancer research [9]. Such precision targeting via therapeutic devices will reduce treatment side effects, resulting in better patient compliance.

This novel technique relies on generating thrust on a magnetic device, containing therapeutical solution, using the magnetic force related to the gradients of the MRI magnetic field. Not only does MRI device provide propelling energy, but accurate observation capability, thanks to control and imaging multiplexing approach [11].

Because the tiniest capillaries are in the 5-6 micron range, the robot should be in the range of 10-100 nanometers [2] to avoid embolization and to drive the drugs as close as possible to the tumor. Analysis on the force capabilities of clinical MRI systems shows that it is impossible to steer nanoscale robots in arteries. An optimal ratio between robot's and vessel's radii, evocated in [9], should be respected. A way to overcome the MRI limitations is to make the radius of the robot decrease as it goes in smaller vasculature. This can be done if the robot is a polymer binded aggregate of magnetic particles, loosing substance with time.

This paper proposes a precise model of a robot in blood vessels including wall effects (parabolic profile of blood flow, pulsatile vessel walls), wall interactions (Van der Waals, electrostatic and contact forces) and non-Newtonian behavior of blood (Section II). This model points out the importance of wall interactions, often neglected, in the determination of an optimal trajectory (Section III) which minimize significantly the control efforts. A backstepping control approach [8] [6] is used to ensure a stabilization along any desired trajectory. The performance and the stability of the closed loop system with respect to noise measurement and parameters variations are illustrated by simulations (Section IV). Finally, we sum up results and discuss prospects (Section V).

II. MODELING

The purpose of this section is to present a 2D highly nonlinear model for a polymer binded aggregate of ferro-magnetic (NdFeB) particles immersed in blood vessel. The model encompasses the different forces that affect the robot's motion as well as its interaction with the vessel wall. The translational of the robot is expressed by:

$$m\frac{d\vec{v}}{dt} = \vec{F}_m + \vec{F}_d + \vec{W}_a + \vec{F}_c + \vec{F}_{vdw} + \vec{F}_{elec} \qquad (1)$$

where $\vec{v}$ is the translational velocity of the robot and m its mass. $\vec{F}_m$, $\vec{F}_d$, $\vec{W}_a$, $\vec{F}_c$, $\vec{F}_{vdw}$ and $\vec{F}_{elec}$ respectively denote the magnetic force produced by the MRI gradient coils, blood hydrodynamic drag force, apparent weight, the robot-to-wall contact force, the Van der Waals and the electrostatic force.

In the rest of this paper, we assume that the orientation of the robot does not change due to the magnetic torque which tends to align the magnetization of the robot along the external field. We also assume that the robot is large enough to neglect the effect of Brownian motion.

A. Magnetic force

The gradient coils of the MRI system provide magnetic gradients which produce a magnetic force F_m on the robot:

$$\vec{F}_m = \tau_m \mu_0 V(\vec{M}.\nabla)\vec{H} \qquad (2)$$

This work was supported by European Union's 7th Framework Program and its research area ICT-2007.3.6 Micro/nanosystems under the project NANOMA (Nano-Actuactors and Nano-Sensors for Medical Applications).

L. Arcese and M. Fruchard are with the Institut PRISME UPRES 4229, IUT de Bourges, 63 Av de Lattre de Tassigny, 18020, Bourges cedex, France laurent.arcese@bourges.univ-orleans.fr matthieu.fruchard@bourges.univ-orleans.fr

A. Cherry and A. Ferreira are with the Institut PRISME UPRES 4229, ENSI de Bourges, 88 Bd Lahitolle, 18000, Bourges, France ali.cherry@ensi-bourges.fr antoine.ferreira@ensi-bourges.fr

where V is the robot's total volume, $\tau_m = \frac{V_m}{V}$ with V_m the ferromagnetic volume, $\vec{M}$ is the magnetization of the material, μ_0 is the permeability of free space, $\vec{H}$ is the external magnetic field, and ∇ is the gradient operator.

B. Hydrodynamic drag force

The hydrodynamic drag force $\vec{F}_d$ exerting on a spherical body is expressed as:

$$\vec{F}_d = -\frac{1}{2}\rho_f \left[\frac{\|(\vec{v}-\vec{v}_f)\|}{\beta}\right]^2 AC_d \frac{(\vec{v}-\vec{v}_f)}{\|(\vec{v}-\vec{v}_f)\|} \quad (3)$$

where $\vec{v}-\vec{v}_f$ denotes the relative velocity of the robot with respect to the fluid, A is the frontal area of the core and ρ_f is the density of the fluid.

For endovascular applications, influence of the vessel walls on the velocity of the robot has to be taken into account. In general, this wall effect is expressed as [7]:

$$\beta = \frac{1+\left(\frac{\lambda}{\lambda_0}\right)^{\alpha_0}}{1-\lambda^{\alpha_0}}$$

with ratio $\lambda = 2r/D$ and D denoting the vessel diameter (in meter). Parameters α_0 and λ_0 are functions of Reynolds number, but are commonly set to 1.5 and 0.29, respectively. The drag coefficient C_d, which is a function of the Reynolds number, is given by [13]:

$$C_d = \frac{24}{Re} + \frac{6}{1+\sqrt{Re}} + 0.4$$

with Re denoting the Reynolds number:

$$Re = \frac{2r\rho_f\,|\vec{v}-\vec{v}_f|}{\beta\eta}$$

In the case of blood, which exhibits a non-newtonian behavior, the fluid's viscosity η is a function of vessel diameter d (in micron) and hematocrit rate h_d according to the following empirical relations [10]:

$$\eta = \frac{\eta_{plasma}d^2}{(d-1.1)^2}\left[1+\frac{(\eta_{0.45}-1)d^2}{(d-1.1)^2}\frac{(1-h_d)^c-1}{(1-0.45)^c-1}\right]$$

with parameters η_{plasma} and $\eta_{0.45}$ denoting respectively the plasma's viscosity and the relative apparent blood viscosity for a fixed discharge hematocrit of 0.45, given by:

$$\eta_{0.45} = 6\,e^{-0.085d} + 3.2 - 2.44\,e^{-0.06d^{0.645}}$$

The shape of the viscosity dependance on hematocrit is:

$$c = \frac{10^{11}}{d^{12}} - (0.8+e^{-0.075d})\left(\frac{d^{12}}{d^{12}+10^{11}}\right)$$

Wall effects on the fluid in a vessel traditionally result in a parabolic profile of blood flow (see Figure 1). Besides, to fully take into account pulsatile flow caused by heart pumping in arteries, one has to consider a periodic deformation of the vessel's diameter $D(t)$ synchronized with the pulsative blood velocity $v_f(t)$.

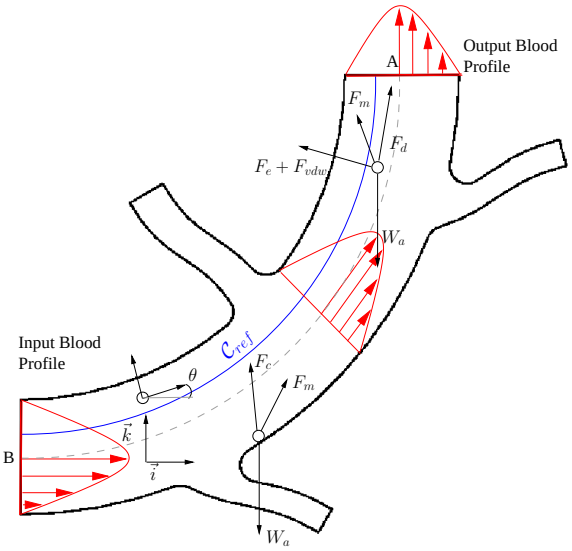

Fig. 1. Scheme of a blood vessel with minor bifurcations

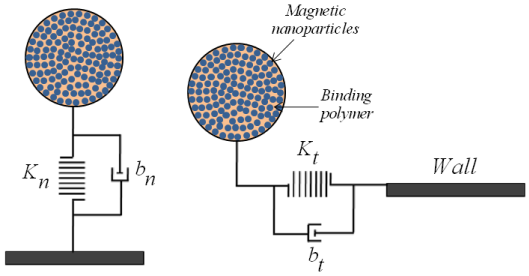

Fig. 2. Model of contact forces: robot-to-wall

C. Apparent weight

In addition to the magnetic and hydrodynamic forces, apparent weight (combined action of weight and buoyancy) is acting on the spherical robot:

$$\vec{W}_a = V(\rho-\rho_f)\vec{g} \quad (4)$$

where $\rho = \tau_m\rho_m + (1-\tau_m)\rho_{poly}$ with ρ_m and ρ_{poly} the magnetic material's and polymer's densities.

D. Contact force

The normal and tangential interactions between the robot and the wall are assumed to be expressed by a Voigt model (see figure 2), where the spring constant K and the decay coefficient of dashpot b are functions of Young's modulus E and Poisson's ratio σ [12].

The normal component of the contact force $\vec{F}_{cn}$ acting on the robot is given by:

$$\vec{F}_{cn} = (K_n\delta^{3/2} + b_n\dot{\delta})\vec{n} \quad (5)$$

where δ is the elastic deformation of the wall at the contact point and $\vec{n}$ is the normal unit vector pointing from the robot to the contact surface.

The tangential component of the contact force takes part when the robot is rotating or in case of oblique collision with the wall:

$$\vec{F}_{ct} = (K_t\zeta + b_t\dot{\zeta})\vec{t} \tag{6}$$

where ζ is the displacement in the tangential direction and $\vec{t}$ is the tangential unit vector.

E. Van der Waals and electrostatic forces

When the robot and the wall are not in contact, they interact each other through Van der Waals and electrostatic forces. The Van der Waals potential between the robot and the wall is given by [5]:

$$\vec{V}_{vdw} = -\frac{A_h}{6}\left(\frac{1}{h} + \frac{1}{2+h} + \ln\frac{h}{2+h}\right)\vec{n} \tag{7}$$

where A_h is the Hamaker constant and h is the distance between the robot and the wall. Then, the Van der Waals interaction force is given by differenciating (7):

$$\vec{F}_{vdw} = -\nabla\vec{V}_{vdw} \tag{8}$$

The electrostatic force between the robot and the wall considered as an uncharged surface is given by [3]:

$$\vec{F}_{elec} = \frac{q^2}{4\pi\epsilon\epsilon_0(r+h)^2}\vec{n} \tag{9}$$

with q the robot charge, ϵ the dielectric density of the medium in which the interaction occurs and ϵ_0 the vacuum permittivity. [4] gives the expression of the maximum allowable charge for a spherical body of radius r:

$$q(\mu C) = S \times Q = 4\pi r^2 \times 30(100r)^{-0.3}$$

III. Optimal trajectory and control approach

Previous forces balance gives us sufficient informations to plan an optimal trajectory. At least two positions A and B, shown on the Figure 1, should be taken into account. In the first one, the robot is in a vertical vessel and the magnetic force $\vec{F}_m$ should counter both contributions of the robot's apparent weight $\vec{W}_a$ and the drag force $\vec{F}_d$ when blood is flowing back (Curve A of Figure 3). The drag force decreases when the robot approaches the wall due to the parabolic profile of velocity. Thus the reference trajectory should be near the wall.

In the second case, the robot is in a horizontal vessel and the magnetic force should counter contributions of the robot's apparent weight, electrostatic and Van der Waals forces, $\vec{F}_{elec}$ and $\vec{F}_{vdw}$ (Curve B of Figure 3). This case shows that near the wall, $\vec{F}_{elec}$ and $\vec{F}_{vdw}$, which point to the wall, are dominant and the magnetic force is no more sufficient to counter it. Nevertheless there is an optimal position where the sum of the two forces compensates perfectly the robot's weight. Moreover, the curve A shows that at this point, the magnetic force exceeds the drag force.

From these observations, we define an optimal path as an arc passing through the point C. A backstepping control approach have been developed in order to ensure a null error between real and desired trajectory. The reader may refer to [1] for details on the control approach.

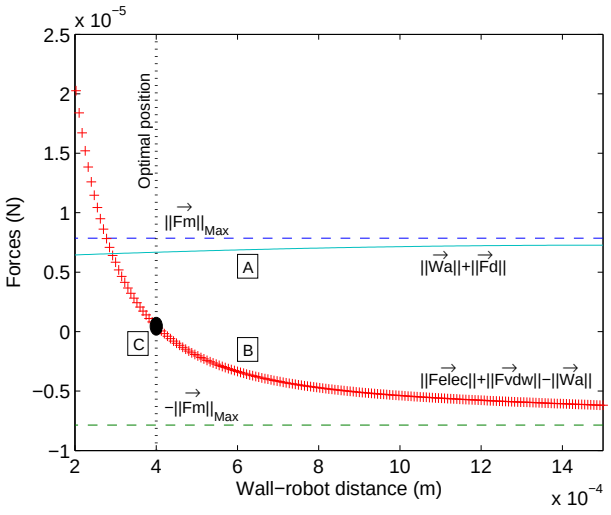

Fig. 3. Forces balances in vertical (A) and horizontal (B) artery

IV. Simulations

Simulations are performed by taking into account the limitations of a clinical MRI system. The pulsative blood's velocity is modeled by an affine combination of a time-varying periodic flow with a spatial parabolic shape. So as to simplify the analytical expression, but with no loss of generality, we only consider the first terms in the time-varying Fourier series of the physiological pulse. In the case of an artery, such an approximation leads to:

$$v_f(t) = 0.025(1 + 1.15\sin 2\pi t) \times \left[1 - \left(\frac{D/2 - h}{r}\right)^2\right]$$

Our studies assume the presence of minor bifurcations (see Figure 1). The developed controller must be sufficiently robust to compensate this effect which could be considered as a disturbance. Major bifurcations will require a further study of velocity's field profile.

In the following, the performances and stability of the controller with respect to noise measurement, parameters variations and uncertainties are illustrated by a simulation, whose parameters are given in Table I. The simulation is performed by assuming that the blood's viscosity and permittivity are affected by uncertainties of 100% of their nominal values and the vessel's diameter by uncertainties of 10%. Besides, a white gaussian noise about 10% of the measured signal is applied on the position measurement.

This simulation shows that after a transient phase (see figure 4), the position tracking performance is robust enough to model's error, but proved quite sensitive to output noise, though remains stable. Despite these uncertainties and disturbances, Figure 5 shows that the control inputs do not reach

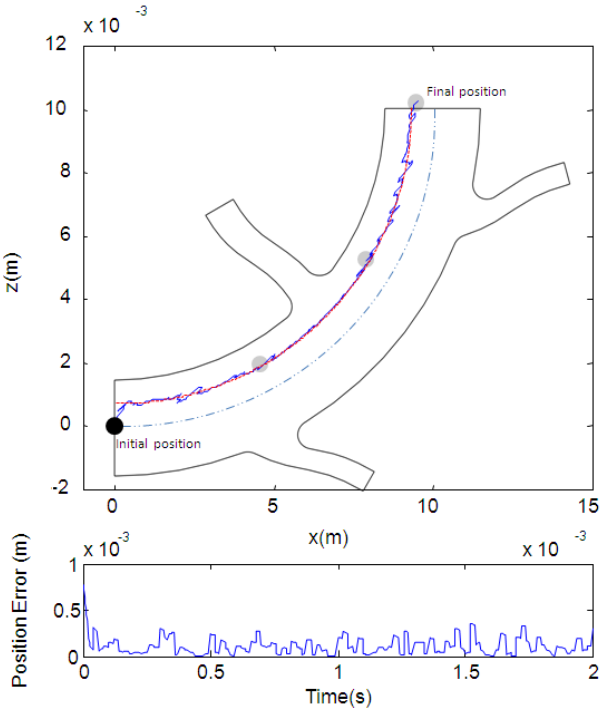

Fig. 4. XZ trajectory : reference trajectory (red dotted) and real trajectory (blue solid line)

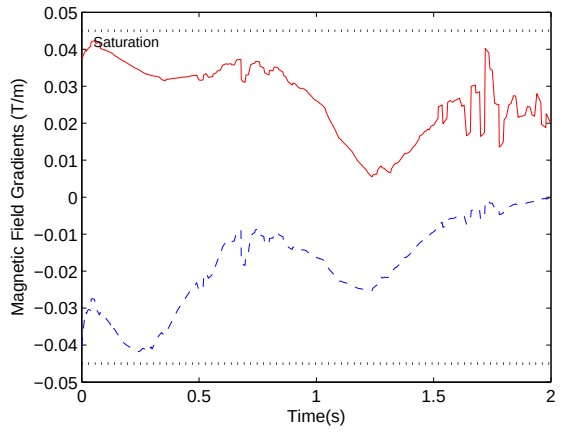

Fig. 5. Control input : magnetic field gradients on $\vec{i}$-axis (dotted) and on $\vec{k}$-axis (solid line)

saturation. This is due to the choice of an optimal reference trajectory deduced from the analysis of Section III.

V. Conclusion

In this paper, we have developed a highly nonlinear model for a MRI guided microrobot in blood vessels with minor bifurcations. This model takes into account the non-newtonian behavior of blood, as well as wall effects and interactions. It makes it possible to hence deduce an optimal trajectory. A backstepping approach have been used to follow desired trajectory. Parameters uncertainties and noise effects have been illustrated by simulation. It appears that the system is robust to uncertain physiological parameters, but proved quite sensitive to output noise, though remains stable. Actually, we are working on the estimation of the blood's velocity and frequency, assumed to be known in the present simulation. The modeling of the impact of major bifurcations on the blood's velocity profile is also underway.

TABLE I

Simulations data

Plasma's viscosity	η_{plasma}	5×10^{-3} $[Pa.s]$
Blood's density	ρ_f	1060 $[kg.m^{-3}]$
Robot's density	ρ_m	8000 $[kg.m^{-3}]$
Robot's radius	r	300 $[\mu m]$
Vessel's diameter	D	3 $[mm]$
Polymer's density	ρ_{poly}	1500 $[kg.m^{-3}]$
Ferromagnetic ratio	τ_m	0.8
Magnetization	M	1.95×10^6 $[A.m^{-1}]$
Hematocrit	h_d	0.45
Robot's Young's modulus	E_p	10^9 $[Pa]$
Wall's Young's modulus	E_w	0.75×10^6 $[Pa]$
Robot's Poisson's ratio	σ_p	0.27
Wall's Poisson's ratio	σ_w	0.30
Hamaker constant	A_h	4×10^{-19} $[J]$
Blood's dielectric density	ε	77 $[C^2.N^{-1}.m^{-2}]$
Inputs saturations	$u_{i,max}$	45 $[mT.m^{-1}]$

References

[1] L. Arcese, M. Fruchard, and A. Ferreira, "Nonlinear modeling and robust controller-observer for a magnetic microrobot in a fluidic environment using mri gradients," *IEEE International Conference on Intelligent Robots and Systems*, pp. 534–539, 2009.

[2] R. Bawa, "Nanoparticle-based therapeutics in humans : A survey," *Nanotechnology Law & Business*, vol. 5:(2), pp. 135–155, 2008.

[3] D. Hays, "Electrostatic adhesion of non-uniformly charged dielectric sphere," *Int. Phys. Conf. ser.*, vol. 118, p. 223228, 1991.

[4] ——, *Role of Electrostatics in Adhesion, in Fundamentals of Adhesion*, L.-H. Lee, Ed. PLENUM PRESS, 1991.

[5] K. Iimura, S. Watanabe, M. Suzuki, M. Hirota, and K. Higashitani, "Simulation of entrainment of agglomerates from plate surfaces by shear flows," *Chemical Engineering Science*, vol. 64, pp. 1455–1461, 2009.

[6] I. Kanellakopoulos, P. Kokotović, and A. Morse, "A toolkit for nonlinear feedback design," *SCL*, vol. 18, pp. 83–92, 1992.

[7] R. Kehlenbeck and R. D. Felice, "Empirical relationships for the terminal settling velocity of spheres un cylindrical columns," *Chemical Eng. Technology*, vol. 21, pp. 303–308, 1999.

[8] M. Krstić, I. Kanellakopoulos, and P. Kokotović, *Nonlinear and Adaptative Control Design*. John Wiley & Sins, Inc., New York, 1995.

[9] J.-B. Mathieu, G. Beaudoin, and S. Martel, "Method of propulsion of a ferromagnetic core in the cardiovascular system through magnetic gradients generated by an mri system," *IEEE Trans. on Biomedical Engineering*, vol. 53, no. 2, pp. 292–299, 2006.

[10] A.-R. Pries, T.-W. Secomb, and P. Gaehtgens, "Biophysical aspects of blood flow in the microvasculature," *Cardiovascular Research*, vol. 32(4), pp. 654–667, 1996.

[11] S. Tamaz, R. Gourdeau, A. Chanu, J.-B. Mathieu, and S. Martel, "Real-time mri-based control of a ferromagnetic core for endovascular navigation," *IEEE Trans. on Biomed. Eng.*, vol. 55, no. 7, July 2008.

[12] Y. Tsuji and T. Tanaka, T. Ishida, "Lagragian numerical simulation of plug flow of cohesionless particles in a horizontal pipe," *Powder Technology*, vol. 71, pp. 239–250, 1992.

[13] F. White, *Viscous Fluid Flow*. McGraw Hill New-York, 1991.